NANO LETTERS
Cite This: Nano Lett. 2019, 19, 6315−6322
Letter
pubs.acs.org/NanoLett

# Stable, Strongly Emitting Cesium Lead Bromide Perovskite Nanorods with High Optical Gain Enabled by an Intermediate Monomer Reservoir Synthetic Strategy

Sheng Wang,[†,○] Jiahao Yu,[‡,○] Minyi Zhang,[§,○] Dechao Chen,[⊥] Chunsen Li,[§] Rui Chen,[*,‡] Guohua Jia,[*,⊥] Andrey L. Rogach,[*,¶] and Xuyong Yang[*,†]

[†]Key Laboratory of Advanced Display and System Applications of Ministry of Education, Shanghai University, 149 Yanchang Road, Shanghai 200072, China

[‡]Department of Electrical and Electronic Engineering, Southern University of Science and Technology, Shenzhen, Guangdong 518055, China

[§]State Key Laboratory of Structural Chemistry, Fujian Institute of Research on the Structure of Matter, Chinese Academy of Sciences, Fuzhou, Fujian 350002, China

[⊥]Curtin Institute of Functional Molecules and Interfaces, School of Molecular and Life Sciences, Curtin University, Perth, Western Australia 6845, Australia

[¶]Department of Materials Science and Engineering and Centre for Functional Photonics (CFP), City University of Hong Kong, 83 Tat Chee Avenue, Kowloon, Hong Kong S.A.R.

*S* *Supporting Information*

**ABSTRACT:** One-dimensional (1D) semiconductor nanorods are important for numerous applications ranging from optics and electronics to biology, yet the direct synthesis of high-quality metal halide perovskite nanorods remains a challenge. Here, we develop an intermediate monomer reservoir synthetic strategy to realize the controllable growth of uniform and low-defect $CsPbBr_3$ perovskite nanorods. Intermediates composed of $CsPb_2Br_5$ and $Cs_3In_2Br_9$ are obtained through the substitution of $Pb^{2+}$ with $In^{3+}$ cations in the template of $CsPbBr_3$ nanocubes and act as a precursor reservoir to gradually release monomers, ensuring both the slow growth rate and low defects of nanorods. We have used branched tris(diethylamino)phosphine as a ligand, which not only has unequal binding energies with different crystal faces to promote the orientation growth but also provides strong steric hindrance to shield the nanorods in solution. Because of minor amount of defects and an effective ligand passivation, in addition to significantly enhanced stability, the perovskite nanorods show a high photoluminescence quantum yield of up to 90% and exhibit a net mode gain of 980 $cm^{-1}$, the latter being a record value among all the perovskite materials. An extremely low amplified spontaneous emission threshold of 7.5 $\mu J$ $cm^{-2}$ is obtained under excitation by a nanosecond laser, which is comparable to that obtained using femtosecond lasers in other recent studies.

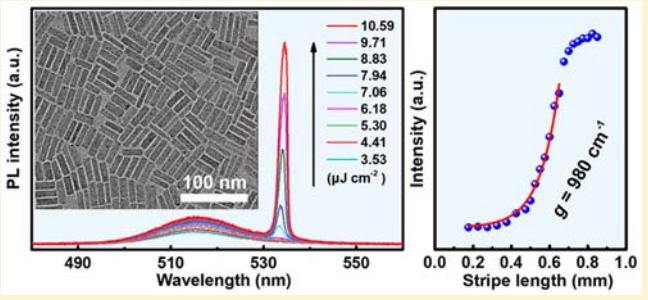


**KEYWORDS:** *Cesium lead bromide perovskites, nanorods, amplified spontaneous emissions, high mode gain, intermediate monomers*

Perovskite nanocrystals (PNCs) with tunable emission wavelengths, narrow emission line widths, high photoluminescence quantum yield (PLQY), and broad optical gain spectrum have been envisioned as promising materials in a wide range of applications such as biological probes, light-emitting diodes, photovoltaics, lasers, and photodetectors.[1−8] Given that the performance of nanocrystals in general has a strong correlation with their shape, the morphology control of PNCs has become a central topic of recent studies.[9−13] For example, one-dimensional (1D) perovskite nanorods have larger photon absorption cross-sections and lower nonradiative recombination rates compared with their counterparts such as traditional nanocubes or spherical nanoparticles, which enable them to stand out in terms of realization of amplified spontaneous emission (ASE).[2,14,15]

However, a direct synthesis of high-quality perovskite nanorods is a subject to three primary limitations. First, metal halide perovskites are ionic compounds so that strong interactions between cations and anions of the precursor materials commonly used for their synthesis lead to an ultrafast nucleation and growth rate,[16−18] which limit the controllability of both morphology and size.[18] Second, slow crystal growth is

**Received:** June 15, 2019
**Revised:** August 17, 2019
**Published:** August 23, 2019





DOI: 10.1021/acs.nanolett.9b02436
Nano Lett. 2019, 19, 6315−6322

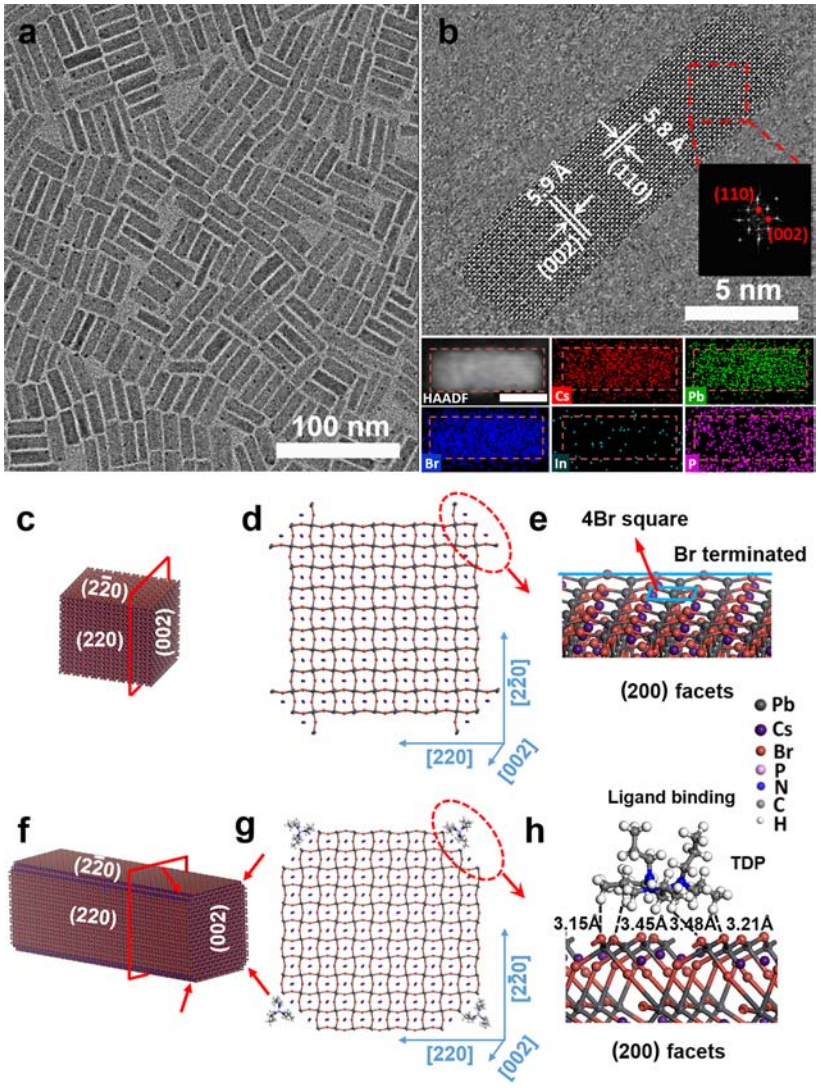


**Figure 1.** (a) TEM image of $CsPbBr_3$ nanorods. (b) HRTEM (top) and HAADF image (scale bar, 10 nm) of a single nanorod, and the corresponding elemental mapping images (bottom). The insert reveals the FFT pattern taken from a selected area of a nanorod. (c) Schematics of a $CsPbBr_3$ nanocube with (220), (2$\bar{2}$0), and (002) facets being the surface facets. (d) Projection of the crystal lattice viewing from the [002] direction. (e) Br-terminated surface structure of the (200) facet as marked by the dashed ellipse in panel d. The cyan-blue rectangle in panel e indicates a part of the surface where each four Br atoms form a 4Br square. (f) Schematics of a $CsPbBr_3$ nanorod. Four arrows indicate that the surface Br atoms on the (200) facets are passivated by TDP ligand. (g) Projection of the crystal lattice viewing from the [002] direction. (h) TDP ligand binding on the (200) facet as marked by the dashed ellipse in (g). Dashed lines in panel h indicate the formation of hydrogen bonds.

beneficial for high crystallinity nanocrystals, whereas ultrafast growth rate can inevitably result in a high defect density and thus decrease PLQYs and diminish ASE prospects.[19−24] Third, instability of metal halide perovskites needs to be addressed and improved for a proper ASE realization.[25,26] Most of the previously reported synthetic pathways toward perovskite nanorods have been thus enabled via ligand-induced fragmentation of perovskite nanowires[23] or chemical transformation from $Cs_4PbBr_6$ nanopolyhedrons at the water−oil interface.[24] However, oleic acid (OA) and oleylamine (OAm), which are commonly used as the ligands of the nanorods mentioned earlier, are too labile to support the good stability of PNCs,[27−29] and the abundant defects in the template nanowires or degradation of water molecules during the transformation of $Cs_4PbBr_6$ nanocrystals deteriorate their emission efficiencies.

In this work, we developed a novel synthetic strategy, which we denote as an intermediate monomer reservoir synthesis, to simultaneously allow for the formation of highly uniform, low-defect, and stable $CsPbBr_3$ nanorods with high PLQY of 90%. The cation exchange between $Pb^{2+}$ ions in original $CsPbBr_3$ nanocubes and the $In^{3+}$ ions introduced in solution results in the formation of intermediates composed of $CsPb_2Br_5$ and $Cs_3In_2Br_9$. Cs and Br precursors can be gradually released from these intermediates at elevated temperatures and thus continuously compensate for the monomer consumption, which ensures slow growth of $CsPbBr_3$ PNCs allowing sufficient time for the crystallization. Assisted by branched tris(diethylamino)phosphine (TDP) ligand, a 1D oriented growth results in the formation of $CsPbBr_3$ nanorods with high PLQY and sufficient stability, which benefits from the branched TDP structure providing excellent passivation and strong steric hindrance.[27,30] Furthermore, we demonstrate a record gain value of 980 $cm^{-1}$, and a very low ASE threshold of 7.5 $\mu J$ $cm^{-2}$ for these $CsPbBr_3$ nanorods under optical



DOI: 10.1021/acs.nanolett.9b02436
Nano Lett. 2019, 19, 6315−6322

pumping by a nanosecond laser, instead of a high energy femtosecond laser.

Pristine $CsPbBr_3$ nanocubes (Figure S1a) are presynthesized using a modified hot-injection synthetic approach by adding oleylammonium bromide to achieve a stoichiometric reaction.[31] Nanocubes have a uniform size distribution with an average edge length of ∼11.2 nm, and their high-resolution TEM (HRTEM) and elemental mapping images (Figure S2) indicate distinct lattice fringes and homogeneous distribution of Cs, Pb, and Br elements. As revealed by the powder X-ray diffraction (XRD) patterns (Figure S3), pristine $CsPbBr_3$ nanocubes have an orthorhombic crystal structure. Next, $In(OAm)_3$ and TDP are added to the crude solution of $CsPbBr_3$ nanocubes to initiate the transition from $CsPbBr_3$ nanocubes to $CsPbBr_3$ nanorods. The analysis of XRD patterns of the reaction products taken under different heating stages shows that this transition is temperature-dependent (Figure S3) and reversible (Figure S4). When the temperature of the mixture is increased to 50 °C, bright green solution becomes colorless, and the TEM image taken at this stage shows that $CsPbBr_3$ nanocubes convert into a mixture of truncated cubes and spheres (Figure S1b). The XRD pattern of the reaction products (Figure S3) can be indexed as a mixture of $Cs_3In_2Br_9$ and $CsPb_2Br_5$ (denoted as intermediates in the follow-up discussion), which is further confirmed by combining HRTEM with fast Fourier transform (FFT) analysis (Figure S5). The transformation from $CsPbBr_3$ to $Cs_3In_2Br_9$ is possible because the bond energy of In−Br (318.6 kJ/mol) is 27% larger than that of Pb−Br (249 kJ/mol);[32,33] such a large disparity in bond energies favors the replacement reaction of the $Pb^{2+}$ by the $In^{3+}$ cations. Meanwhile, $CsPb_2Br_5$ is favored in a lead-rich phase,[34] and the abundant substituted $Pb^{2+}$ ions promote the transformation from $CsPbBr_3$ to $CsPb_2Br_5$. With a further increase of the temperature from 50 to 80 °C, the colorless solution gradually becomes green. The diffraction peaks of the intermediates become weaker, and several new diffraction peaks corresponding to $CsPbBr_3$ NCs reappear (Figure S3).

The corresponding TEM image shown in Figure S1c presents $CsPbBr_3$ nanorods with a diameter of ∼5.8 nm and a length of ∼26 nm, together with quasi-spherical intermediate particles. XRD patterns taken at this stage (Figure S3) confirm the partial decomposition of intermediates and recrystallization of $CsPbBr_3$ nanorods. The temperature-dependent conversion of the intermediates is further confirmed by the XRD patterns of reaction products obtained by cycling the reaction temperature from 50 to 100 °C (Figure S4). The intermediates transform to $CsPbBr_3$ nanorods at 100 °C, which can retransform back to the intermediates when the temperature cools down to 50 °C. Apparently, intermediates are less stable at higher temperature, and release Cs and Br precursors, which are coordinated with the abundant $Pb^{2+}$ to form $CsPbBr_3$ PNCs. When the temperature reaches 100 °C, the (002) and (004) diffraction peaks of the reaction product (nanorods) are significantly narrowed and enhanced in comparison to those of the pristine $CsPbBr_3$ nanocubes, and the diffraction peaks corresponding to intermediates vanish. This corroborates that intermediates are completely decomposed and transform into nanorods with the long axis being parallel to the [002] direction.[35] The obtained $CsPbBr_3$ nanorods are rather monodisperse, with an increased diameter of ∼8.5 nm and the length of ∼30 nm (Figures 1a and S6a). This is different from the nanorods produced through ligand-induced fragmentation of nanowires[23] and chemical transformation from $Cs_4PbBr_6$ nanopolyhedrons,[24] which kept almost identical diameters within the whole reaction process, while the diameter of nanorods obtained here through the intermediate monomer reservoir synthesis continuously increases. This observation further proves that the $CsPbBr_3$ nanorods are formed through a recrystallization process instead of phase transformation process.

The terminated crystal facets and the axial direction of the $CsPbBr_3$ nanorods can be determined from the HRTEM image and the corresponding fast Fourier transform (FFT) pattern of a horizontally aligned nanorod shown in Figure 1b. The derived interplanar spacing of 0.59 nm is consistent with the (002) *d*-spacing of orthorhombic $CsPbBr_3$ structure. This confirms that [002] orientation is parallel to the long axis of the nanorods, and the flat top is the (002) crystallographic facet. This is also consistent with the enhanced and narrowed (002) and (004) diffraction peaks in the XRD pattern of nanorods (Figure S3). The lateral interplanar distance of 0.58 nm corresponds to the spacing of the (110) planes. The high-angle annular dark-field (HAADF) image and the elemental maps of an individual nanoparticle confirm that Cs, Pb, and Br elements are uniformly distributed through a single nanorod (Figure 1b). The signal of In element is very weak within the region of the nanorod, indicating that it is released to reaction solution and is not incorporated into the $CsPbBr_3$ crystal lattice. The uniform distribution of the P element originates from the TDP ligands densely bound at the surface of the $CsPbBr_3$ nanorod. Slow evaporation of a highly concentrated $CsPbBr_3$ nanorod solution in hexane enables some of them to become vertically aligned on their flat tops; the TEM image of such nanorods (Figure S6b) shows that they have a corner-truncated rectangular cross-section, and the corresponding HRTEM image (the inset in Figure S6b) further confirms that the side surfaces of nanorods are (220) and $(2\bar{2}0)$ crystal facets.

To elucidate the growth mechanism of $CsPbBr_3$ nanorods, and in particular to reveal how $CsPbBr_3$ undergo anisotropic growth under our reaction conditions, we perform the first-principles calculations based on the density-functional theory (DFT)[36−38] to study the surface energy of (002), (220), and (200) facets, which are relevant to crystal growth, and the binding of these facets with TDP ligands (see Supporting Information for details). A schematic of a $CsPbBr_3$ nanocube is shown in Figure 1c. The projection of the crystal lattice viewing from the [002] direction indicates that the $(2\bar{2}0)$ facets are equivalent to the (220) facets (Figure 1d). The (200) facets are Br terminated, and each of the four Br atoms on these facets forms a 4Br square (Figure 1e). Calculations show that the surface energies of (002) and (220) facets are almost the same, being 0.0073 eV/Å$^2$ and 0.0072 eV/Å$^2$, respectively, and both are much lower than that of the (200) facets (0.0246 eV/Å$^2$) (Figure S7). Therefore, the (220) and $(2\bar{2}0)$ facets are the dominant facets, which determine the final morphology of the $CsPbBr_3$ PNCs. In such a case, $CsPbBr_3$ would grow into cubic shaped particles terminated by the (002), (220), and $(2\bar{2}0)$ facets. On the other hand, due to the large surface energy of the (200) facet, the initial epitaxial growth along the [220] direction would be induced by the edges or protrusions toward the [200] direction (Figure 1e). Such a process is followed by the sideward growth along the $[220]/[2\bar{2}0]$ direction, which forms a new layer terminated by $(220)/(2\bar{2}0)$ facets. Thus, the edges or protrusions toward the



DOI: 10.1021/acs.nanolett.9b02436
*Nano Lett.* 2019, 19, 6315−6322

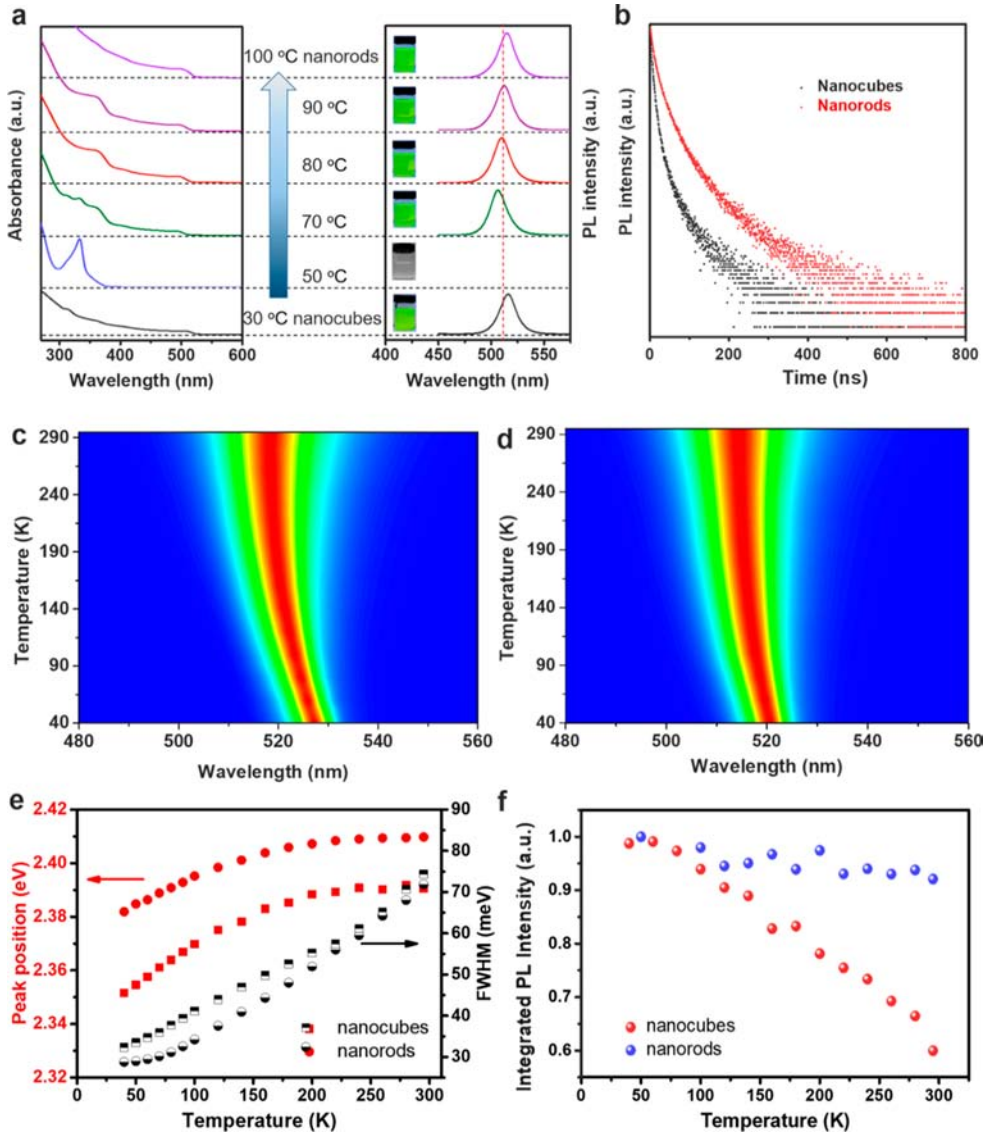


**Figure 2.** (a) Temporal evolution of absorption (left) and PL (right) spectra, with the corresponding optical photographs taken during different stages of the heating reaction. (b) Time resolved PL decays of $CsPbBr_3$ nanocubes and nanorods. Temperature-dependent PL spectra of (c) $CsPbBr_3$ nanocubes and (d) $CsPbBr_3$ nanorods. The samples are excited under 325 nm by a continuous-wave He−Cd laser. (e) PL peak energy and line widths of the two samples as a function of temperature. (f) Temperature dependence of normalized integrated PL intensity for the two $CsPbBr_3$ samples.

[200] direction would play an important role in inducing the growth along the [220] direction.

Figure 1f shows the schematics of a $CsPbBr_3$ nanorod, and the projection of the crystal lattice viewing from the [002] direction is depicted in Figure 1g. Calculations show that TDP ligands have similar binding on both (220) and (002) facets, as the binding energies on these facets are almost the same, that is, −0.26 eV for (002) PbBr, −0.21 eV for (002) CsBr, −0.24 eV for (220) PbBr, and −0.21 eV for (220) CsBr (Table S1 and Figure S8). However, TDP has the lowest binding energy (−0.48 eV) on the (200) facets (about 0.24 eV lower than on that of any other surfaces). Thus, a Br-ion terminated surface structure would form on the relaxed (200) facets due to the enhanced electrostatic interactions between the alkyl hydrogen atoms of TDP ligands and Br ions (Figure 1h). Furthermore, the four hydrogen atoms of the alkyl group of TDP can interact with the nearest four Br ions of the (200) surface (Figure 1e), forming strong ligand adsorption states on the (200) facets (Figure 1h). In this case, the initial epitaxial growth along the [200] direction would be suppressed by the binding of TDP, after which the growth along the [220] direction would also slow down. Considering similar binding on the (220) and (002) facets as mentioned earlier, the growth rate of $CsPbBr_3$ PNCs along the [002] direction is faster than that along the [220] direction in the presence of TDP ligands. As a result, $CsPbBr_3$ PNCs grow into $CsPbBr_3$ nanorods with the (220) and (002) facets being the dominant surfaces and the [002] being the dominant growth direction.

From the DFT analysis, we conclude that TDP ligands play a crucial role in regulating the growth of $CsPbBr_3$ nanorods. However, just a presence of TDP only, without addition of $In(OAm)_3$ in the reaction mixture, results in the formation of large aggregates (Figure S9). In addition, if $In(OAm)_3$ and TDP are mixed with the Cs, Pb, and Br precursors, no intermediates are formed during the heating process, yielding a mixture containing only a small amount of nanorods (Figure



DOI: 10.1021/acs.nanolett.9b02436
Nano Lett. 2019, 19, 6315−6322

S10). We hypothesize that the abundant Cs, Pb and Br precursors in the reaction solution will trigger the ultrafast crystal growth[20] and weaken the mediation effect of TDP ligand. A series of control experiments is further carried out to investigate the synergistic effect of intermediate's decomposition and TDP mediation. OAm has been proven to be responsible for the phase and morphology transformation.[12]

We find out that in our synthesis, the nanocube solution mixed with OAm only, using identical synthetic conditions as those for the nanorods, experiences a ripening process and results in nanocubes with a broad size distribution (Figure S11). In the absence of TDP, intermediates are still formed at 50 °C, but nanocubes rather than nanorods are obtained at 100 °C (Figure S12). Remarkably, when the intermediates have been prepared followed by addition of TDP, the uniform nanorods are generated (Figure S13). In the synthesis performed using the purified $CsPbBr_3$ nanocube solution, nanorods were still produced (Figure S14). The above results clearly demonstrate that the formation of nanorods involves two steps: first, the intermediates containing $CsPb_2Br_5$ and $Cs_3In_2Br_9$ are formed by cation exchange; second, the intermediates act as a monomer reservoir to gradually release precursors for the nucleation and growth of PNCs in a controlled manner, which occurs as the anisotropic growth and lead to the formation of perovskite nanorods under mediation of TDP ligands.

To investigate the evolution of the surface chemistry of the reaction products, X-ray photoelectron spectroscopy (XPS) is carried out with adventitious C 1s peak referenced to 284.8 eV. As shown in Figure S15, the Pb 4f and Br 3d peaks shift to higher binding energies when the nanocubes evolve into intermediates, which is in accordance with the phase transformation from $CsPbBr_3$ to $CsPb_2Br_5$ and the enhanced Pb−Br interactions.[39] When the nanorods are formed, the structure conversion to $CsPbBr_3$ orthorhombic phase promotes the Pb 4f and Br 3d peaks to shift to lower binding energies, but they still have larger binding energies than those of the nanocubes, which is attributed to surface passivation with TDP ligands.[40] The evolution of the In 3d peak is consistent with the formation and decomposition of $Cs_3In_2Br_9$. The P 2p peak at the binding energies of 130−136 eV[41] confirms the presence of TDP ligands in the intermediates and nanorods.

The formation of $CsPbBr_3$ nanorods from nanocubes is also evident from the changes in UV−vis absorption and PL spectra (Figure 2a). PL maximum of the pristine $CsPbBr_3$ nanocubes locates at 516 nm with a full-width at half-maximum (fwhm) of 17 nm and PLQY of 73%. After addition of $In(OAm)_3$ and TDP at room temperature and then heating to 50 °C, the PL emission disappears, and the absorption wavelength longer than 377 nm disappear as well so that the first exciton peak is located at 333 nm. This is attributed to the ion exchange process leading to the transformation from the original perovskite structure to the intermediates, that is, the mixture of $CsPb_2Br_5$ and $Cs_3In_2Br_9$. $CsPb_2Br_5$ has an approximately 3.1 eV indirect band gap, thereby it is nonemissive, and its absorption spectrum does not show any distinct features,[34] while $Cs_3In_2Br_9$ is a large direct bandgap semiconductor with no absorption in the visible range.[42] Consequently, the intermediates show no PL emission, and their absorption edge close to 380 nm is well in agreement with the indirect bandgap of $CsPb_2Br_5$, while the first exciton peak at 333 nm arises from the intrinsic absorption of $Cs_3In_2Br_9$. As the reaction temperature is increased to 70 °C and above, the emission reappears, and the PL peak wavelength is gradually red-shifted from 505 to 515 nm, which is in accordance with the increase in the diameter of nanorods (Figures 1a and S1c). The PLQYs of $CsPbBr_3$ nanorods also increase gradually, reaching maximum value of 90%. This is mainly ascribed to the fact that the slow growth rate of the nanorods enables favorable atom arrangement,[25] thus resulting in a low density of trap states in the nanorods.

From PL decays shown in Figure 2b, average PL decay lifetimes ($\tau_{ave}$) of the $CsPbBr_3$ nanocubes and nanorods are determined to be 33 and 73 ns, respectively. Longer PL lifetime of the nanorods can be attributed to the reduced nonradiative recombination,[43,44] which is also consistent with their improved PLQYs. Temperature-dependent PL measurements from 40 to 295 K is carried out to further probe the effect on the defect states for the $CsPbBr_3$ nanocube and nanorod samples (Figure 2c,d). It can be clearly seen that the PL peak position is obviously blue-shifted, and the fwhm becomes broader for both samples at elevated temperature (Figure 2e) due to the electron−phonon coupling effect.[25,45−47] Figure 2f shows the normalized integrated PL intensity as a function of temperature from 40 to 295 K. Compared with nanorods, a rapid PL decrease is observed with increasing temperature for the nanocube sample. When the temperature is increased to 295 K, the PL intensity of nanocubes is only 60% of the emission intensity obtained at 50 K, while that of the nanorods still maintains 92%. If the nonradiative recombination channel such as defect trap states would be present, the PL intensity would dramatically reduce as the temperature increases.[48] We conclude that the nonradiative recombination in the $CsPbBr_3$ nanorods is significantly suppressed, making them promising candidates for optoelectronic applications.

For the metal halide perovskites in general, detrimental effects of water and heat have been always considered as a serious issue hindering their practical applications. We have conducted stability tests of the films prepared from pristine $CsPbBr_3$ nanocubes and $CsPbBr_3$ nanorods. As shown in Figure 3a, when the films are immersed in water, the emission of the nanocube film is quenched within 8 min, while the PL intensity of nanorods film still maintains 80% of its original value after 30 min. Film stability under the heating has been evaluated as well; Figure 3b shows that the PL intensity of nanocubes continuously decreases to 15% of its initial intensity when the temperature is increased to 120 °C, while the PL intensity of the nanorod film remains stable (and even slightly increases) at the temperatures up to 90 °C and still maintains 60% of its original PL intensity when heated up to 120 °C. We ascribe such improved stability to the presence of TDP ligands on the nanorod surface, whose branched structure provides stronger steric hindrance than traditional ligands such as OA and OAm (Figure S16), enabling higher stability of $CsPbBr_3$ nanorods both in aqueous and high-temperature environments.[27,30]

To investigate the nonlinear optical properties of $CsPbBr_3$ nanorods, we examine the emission of the samples under optical pumping by a 355 nm nanosecond pulse laser with a pulse width of 1 ns, and repetition rate of 20 Hz. Under identical excitation situation, an obvious ASE emission can be clearly observed from $CsPbBr_3$ nanorods (Figure 4), which is absent for $CsPbBr_3$ nanocubes (Figure S17). It can be seen from Figure 4a that the $CsPbBr_3$ nanorods show spontaneous



DOI: 10.1021/acs.nanolett.9b02436
Nano Lett. 2019, 19, 6315−6322

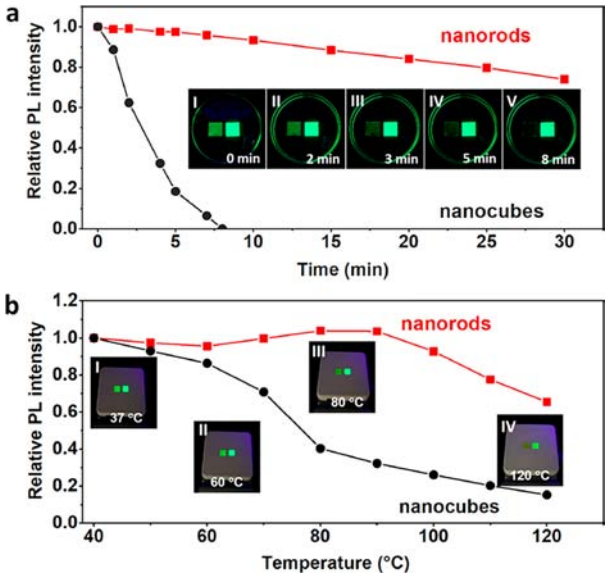


**Figure 3.** Variation of the relative PL intensities of the films made of $CsPbBr_3$ nanocube and nanorod placed in (a) water and on (b) a hot plate. Insets show corresponding optical photographs of the green emitting films made of $CsPbBr_3$ nanocubes (left spot on each photo) and nanorods (right spot on each photo) taken at different treatment stages.

emission with maximum at 516 nm under low excitations. With increasing pump fluence, a sharp emission peak emerges at 534 nm, whose intensity increases rapidly with a raising pump fluence. Figure 4b shows the fwhm of the emission (right *y*-axis) and the integrated PL intensity (left *y*-axis) as a function of pump fluence. The fwhm of the spontaneous emission is about 19 nm, while that of an ASE peak is ∼2 nm. The nonlinear increase of the integrated intensity exhibits a clear threshold behavior, with the threshold at 7.5 $\mu J\ cm^{-2}$, which is at the same level of the best values in recent studies.[7,22,44,49,50] However, it is worth pointing out that the pulse duration (1 ns) of the excitation laser used herein is longer than the time constant of nonradiative Auger recombination (picosecond to hundreds of picoseconds).[49,51−53]

Compared with the femtosecond pulses, the optical pumping by nanosecond laser needs a much larger energy density to compete the Auger recombination for population inversion.[54] Therefore, the threshold of 7.5 $\mu J\ cm^{-2}$ obtained by a nanosecond laser in our work is extremely low compared with those obtained by femtosecond laser reported in previous literature, and which have shown more practical value for applications.[7,55] In addition to the low threshold, the net modal gain is another important figure of merit to evaluate the light amplification ability of materials. Through the variable stripe-length measurement, the gain value of $CsPbBr_3$ nanorods is determined to be 980 $cm^{-1}$ (Figure S18). To the best of our knowledge, this is the highest value among all reported perovskite materials (Table S2). The extremely low threshold of the ASE and the high modal gain make $CsPbBr_3$ nanorods a promising material for laser device applications.

In summary, we developed an intermediate monomer reservoir synthetic strategy that enables gradual monomer release to prepare high-quality $CsPbBr_3$ nanorods with uniform morphology, few defects, and high stability. The obtained $CsPbBr_3$ nanorods have a higher PLQY of 90% compared to the pristine $CsPbBr_3$ nanocubes (73%). Moreover, the nanorods reach a record gain coefficient of 980 $cm^{-1}$ among all perovskite materials and an ultralow ASE threshold of 7.5 $\mu J\ cm^{-2}$ when pumped by a nanosecond laser, which exceeds the best values achieved by using femtosecond laser. This work will open a new avenue in the synthesis of high-quality metal halide perovskite anisotropic nanorods with diverse applications in lasers and other nanoscale optoelectronic devices.

## ■ ASSOCIATED CONTENT

### Supporting Information

The Supporting Information is available free of charge on the ACS Publications website at DOI: 10.1021/acs.nanolett.9b02436.

Additional experimental details; morphology, XRD patterns, and optical spectra evolution of $CsPbBr_3$ nanocrystals on different reaction conditions; XPS spectra of $CsPbBr_3$ nanocubes, intermediates, and $CsPbBr_3$ nanorods; pump fluence-dependent emission of pristine $CsPbBr_3$ nanocubes; modal optical gain of $CsPbBr_3$ nanorods; table of gain values reported for different metal halide perovskites (PDF)

## ■ AUTHOR INFORMATION

### Corresponding Authors

*E-mail: chenr@sustech.edu.cn.

*E-mail: guohua.jia@curtin.edu.au.

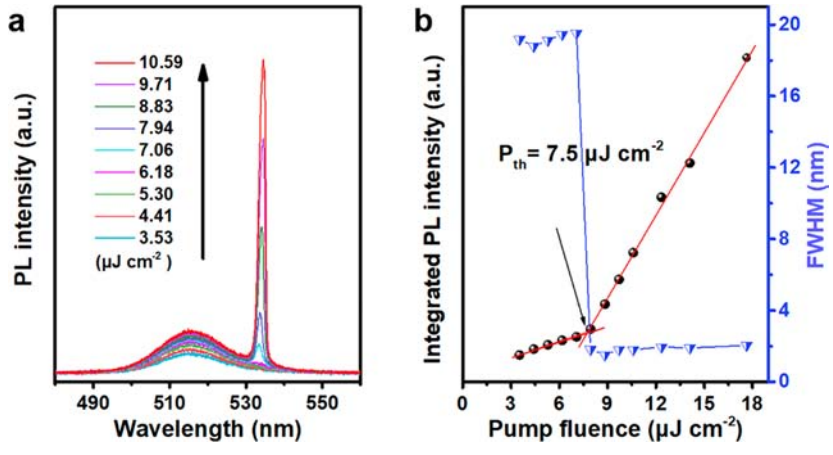


**Figure 4.** (a) Pump fluence-dependent emission. (b) Integrated PL intensity and fwhm as a function of pump fluences.



DOI: 10.1021/acs.nanolett.9b02436
*Nano Lett.* 2019, 19, 6315−6322

*E-mail: andrey.rogach@cityu.edu.hk.
*E-mail: yangxy@shu.edu.cn.

ORCID

Chunsen Li: 0000-0002-9142-0187
Rui Chen: 0000-0002-0445-7847
Guohua Jia: 0000-0003-1179-2763
Andrey L. Rogach: 0000-0002-8263-8141
Xuyong Yang: 0000-0003-3597-1491

### Author Contributions

○S.W., J.Y., and M.Z. contributed equally to this manuscript.

### Notes

The authors declare no competing financial interest.

## ■ ACKNOWLEDGMENTS

The authors acknowledge the financial support from National Natural Science Foundation of China (51675322, 61605109, 61735004), National Key Research and Development Program of China (2016YFB0401702), National Natural Science Foundation of China/Research Grants Council Joint Research Scheme (N_CityU108/17), Shanghai Rising-Star Program (17QA1401600), and The Program for Professors of Special Appointment (Eastern Scholar) at Shanghai Institutions of Higher Learning. G.J. acknowledges the ARC DECRA (Project ID: DE160100589) for financial support.

## ■ REFERENCES

(1) Kovalenko, M. V.; Protesescu, L.; Bodnarchuk, M. I. *Science* **2017**, *358*, 745−750.
(2) Akkerman, Q. A.; Rainò, G.; Kovalenko, M. V.; Manna, L. *Nat. Mater.* **2018**, *17*, 394−405.
(3) Wei, Y.; Deng, X.; Xie, Z.; Cai, X.; Liang, S.; Ma, P.; Hou, Z.; Cheng, Z.; Lin, J. *Adv. Funct. Mater.* **2017**, *27*, 1703535.
(4) Huang, H.; Polavarapu, L.; Sichert, J. A.; Susha, A. S.; Urban, A. S.; Rogach, A. L. *NPG Asia Mater.* **2016**, *8*, e328.
(5) Veldhuis, S. A.; Boix, P. P.; Yantara, N.; Li, M.; Sum, T. C.; Mathews, N.; Mhaisalkar, S. G. *Adv. Mater.* **2016**, *28*, 6804−6834.
(6) Xu, Y.; Chen, Q.; Zhang, C.; Wang, R.; Wu, H.; Zhang, X.; Xing, G.; Yu, W. W.; Zhang, Y.; Xiao, M.; et al. *J. Am. Chem. Soc.* **2016**, *138*, 3761−3768.
(7) Yakunin, S.; Protesescu, L.; Krieg, F.; Bodnarchuk, M. I.; Nedelcu, G.; Humer, M.; Luca, G. D.; Fiebig, M.; Heiss, W.; Kovalenko, M. V. *Nat. Commun.* **2015**, *6*, 8056.
(8) Qiu, T.; Hu, Y.; Xu, F.; Yan, Z.; Bai, F.; Jia, G.; Zhang, S. *Nanoscale* **2018**, *10*, 20963−20989.
(9) Sun, S.; Yuan, D.; Xu, Y.; Wang, A.; Deng, Z. *ACS Nano* **2016**, *10*, 3648−3657.
(10) Zhang, X.; Bai, X.; Wu, H.; Zhang, X.; Sun, C.; Zhang, Y.; Zhang, W.; Zheng, W.; Yu, W. W.; Rogach, A. L. *Angew. Chem.* **2018**, *130*, 3395−3342.
(11) Ye, S.; Zhao, M.; Song, J.; Qu, J. *Nano Res.* **2018**, *11*, 4654−4663.
(12) Almeida, G.; Goldoni, L.; Akkerman, Q.; Dang, Z.; Khan, A. H.; Marras, S.; Moreels, I.; Manna, L. *ACS Nano* **2018**, *12*, 1704−1711.
(13) Xia, Y.; Xia, X.; Peng, H. C. *J. Am. Chem. Soc.* **2015**, *137*, 7947−7966.
(14) Zhou, H.; Yuan, S.; Wang, X.; Xu, T.; Wang, X.; Li, H.; Zheng, W.; Fan, P.; Li, Y.; Sun, L.; Pan, A. *ACS Nano* **2017**, *11*, 1189−1195.
(15) Xing, G.; Liao, Y.; Wu, X.; Chakrabortty, S.; Liu, X.; Yeow, E. K.; Chan, Y.; Sum, T. C. *ACS Nano* **2012**, *6*, 10835−10844.
(16) Koolyk, M.; Amgar, D.; Aharon, S.; Etgar, L. *Nanoscale* **2016**, *8*, 6403−6409.
(17) Huang, H.; Raith, J.; Kershaw, S. V.; Kalytchuk, S.; Tomanec, O.; Jing, L.; Susha, A. S.; Zboril, R.; Rogach, A. L. *Nat. Commun.* **2017**, *8*, 996.
(18) Ran, C.; Xu, J.; Gao, W.; Huang, C.; Dou, S. *Chem. Soc. Rev.* **2018**, *47*, 4581−4610.
(19) Guzelturk, B.; Kelestemur, Y.; Olutas, M.; Delikanli, S.; Demir, H. V. *ACS Nano* **2014**, *8*, 6599−6605.
(20) Wu, Y.; Wei, C.; Li, X.; Li, Y.; Qiu, S.; Shen, W.; Cai, B.; Sun, Z.; Yang, D.; Deng, Z.; Zeng, H. *ACS Energy Lett.* **2018**, *3*, 2030−2037.
(21) Rahimnejad, S.; Kovalenko, A.; Forés, S. M.; Aranda, C.; Guerrero, A. *ChemPhysChem* **2016**, *17*, 2795−2798.
(22) Xing, G.; Mathews, N.; Lim, S. S.; Yantara, N.; Liu, X.; Sabba, D.; Grätzel, M.; Mhaisalkar, S.; Sum, T. C. *Nat. Mater.* **2014**, *13*, 476.
(23) Tong, Y.; Fu, M.; Bladt, E.; Huang, H.; Richter, A. F.; Wang, K.; Müller-Buschbaum, P.; Bals, S.; Tamarat, P.; Lounis, B.; Feldmann, J.; Polavarapu, L. *Angew. Chem.* **2018**, *130*, 16326−16330.
(24) Jing, Q.; Su, Y.; Xing, X.; Lu, Z. *J. Mater. Chem. C* **2019**, *7*, 1854−1858.
(25) Li, J.; Si, J.; Gan, L.; Liu, Y.; Ye, Z.; He, H. *ACS Appl. Mater. Interfaces* **2016**, *8*, 32978−32983.
(26) Aristidou, N.; Sanchez-Molina, I.; Chotchuangchutchaval, T.; Brown, M.; Martinez, L.; Rath, T.; Haque, S. A. *Angew. Chem., Int. Ed.* **2015**, *54*, 8208−8212.
(27) Wu, L.; Zhong, Q.; Yang, D.; Chen, M.; Hu, H.; Pan, Q.; Liu, H.; Cao, M.; Xu, Y.; Sun, B.; Zhang, Q. *Langmuir* **2017**, *33*, 12689−12696.
(28) Yassitepe, E.; Yang, Z.; Voznyy, O.; Kim, Y.; Walters, G.; Castañeda, J. A.; Kanjanaboos, P.; Yuan, M.; Gong, X.; Fan, F.; Pan, J.; Hoogland, S.; Comin, R.; Bakr, O. M.; Padilha, L. A.; Nogueira, A. F.; Sargent, E. H. *Adv. Funct. Mater.* **2016**, *26*, 8757.
(29) Veldhuis, S. A.; Tay, Y. K. E.; Bruno, A.; Dintakurti, S. S. H.; Bhaumik, S.; Muduli, S. K.; Li, M.; Mathews, N.; Sum, T. C.; Mhaisalkar, S. G. *Nano Lett.* **2017**, *17*, 7424−7432.
(30) Luo, B.; Pu, Y. C.; Lindley, S. A.; Yang, Y.; Lu, L.; Li, Y.; Li, X.; Zhang, J. Z. *Angew. Chem., Int. Ed.* **2016**, *55*, 8864−8868.
(31) Protesescu, L.; Yakunin, S.; Bodnarchuk, M. I.; Krieg, F.; Caputo, R.; Hendon, C. H.; Yang, R. X.; Walsh, A.; Kovalenko, M. V. *Nano Lett.* **2015**, *15*, 3692−3696.
(32) Seki, Y.; Watanabe, H.; Matsui, J. *J. Appl. Phys.* **1978**, *49*, 822−828.
(33) Liu, W.; Lin, Q.; Li, H.; Wu, K.; Robel, I.; Pietryga, J. M.; Klimov, V. I. *J. Am. Chem. Soc.* **2016**, *138*, 14954−14961.
(34) Zhu, J.; Di, Q.; Zhao, X.; Wu, X.; Fan, X.; Li, Q.; Song, W.; Quan, Z. *Inorg. Chem.* **2018**, *57*, 6206−6209.
(35) Cho, K. S.; Talapin, D. V.; Gaschler, W.; Murray, C. B. *J. Am. Chem. Soc.* **2005**, *127*, 7140−7147.
(36) Kresse, G.; Furthmüller. *Phys. Rev. B: Condens. Matter Mater. Phys.* **1996**, *54*, 11169.
(37) Blöchl, P. E. *Phys. Rev. B: Condens. Matter Mater. Phys.* **1994**, *50*, 17953.
(38) Perdew, J. P.; Burke, K.; Ernzerhof, M. *Phys. Rev. Lett.* **1996**, *77*, 3865.
(39) Shen, W.; Ruan, L.; Shen, Z.; Deng, Z. *Chem. Commun.* **2018**, *54*, 2804−2807.
(40) Woo, J. Y.; Kim, Y.; Bae, J.; Kim, T. G.; Kim, J. W.; Lee, D. C.; Jeong, S. *Chem. Mater.* **2017**, *29*, 7088−7092.
(41) Koh, W. K.; Bartnik, A. C.; Wise, F. W.; Murray, C. B. *J. Am. Chem. Soc.* **2010**, *132*, 3909−3913.
(42) Xiao, Z.; Du, K. Z.; Meng, W.; Wang, J.; Mitzi, D. B.; Yan, Y. *J. Am. Chem. Soc.* **2017**, *139*, 6054−6057.
(43) Huang, H.; Susha, A. S.; Kershaw, S. V.; Hung, T. F.; Rogach, A. L. *Adv. Sci.* **2015**, *2*, 1500194.
(44) Wang, Y.; Zhi, M.; Chang, Y. Q.; Zhang, J. P.; Chan, Y. *Nano Lett.* **2018**, *18*, 4976−4984.
(45) Li, D.; Wang, G.; Cheng, H. C.; Chen, C. Y.; Wu, H.; Liu, Y.; Huang, Y.; Duan, X. *Nat. Commun.* **2016**, *7*, 11330.
(46) Xing, J.; Liu, X. F.; Zhang, Q.; Ha, S. T.; Yuan, Y. W.; Shen, C.; Sum, T. C.; Xiong, Q. *Nano Lett.* **2015**, *15*, 4571−4577.
(47) Ha, S. T.; Shen, C.; Zhang, J.; Xiong, Q. *Nat. Photonics* **2016**, *10*, 115−121.



DOI: 10.1021/acs.nanolett.9b02436
*Nano Lett.* 2019, 19, 6315−6322

(48) Wu, K.; Bera, A.; Ma, C.; Du, Y.; Yang, Y.; Li, L.; Wu, T. *Phys. Chem. Chem. Phys.* **2014**, *16*, 22476−22481.
(49) Wang, Y.; Li, X.; Song, J.; Xiao, L.; Zeng, H.; Sun, H. *Adv. Mater.* **2015**, *27*, 7101−7108.
(50) Dey, A.; Rathod, P.; Kabra, D. *Adv. Opt. Mater.* **2018**, *6*, 1800109.
(51) Klimov, V. I.; Mikhailovsky, A. A.; McBranch, D. W.; Leatherdale, C. A.; Bawendi, M. G. *Science* **2000**, *287*, 1011−1013.
(52) Klimov, V. I. *Annu. Rev. Phys. Chem.* **2007**, *58*, 635−673.
(53) Wang, Y.; Leck, K. S.; Ta, V. D.; Chen, R.; Nalla, V.; Gao, Y.; He, T.; Demir, H. V.; Sun, H. *Adv. Mater.* **2015**, *27*, 169−175.
(54) Yakunin, S.; Protesescu, L.; Krieg, F.; Bodnarchuk, M. I.; Nedelcu, G.; Humer, M.; Luca, G. D.; Fiebig, M.; Heiss, W.; Kovalenko, M. V. *Nat. Commun.* **2015**, *6*, 8056.
(55) Huang, C. Y.; Zou, C.; Mao, C.; Corp, K. L.; Yao, Y. C.; Lee, Y. J.; Schlenker, C. W.; Jen, A. K. Y.; Lin, L. Y. *ACS Photonics* **2017**, *4*, 2281−2289.



DOI: 10.1021/acs.nanolett.9b02436
*Nano Lett.* 2019, 19, 6315−6322